SIAM J. MATH. ANAL.
Vol. 56, No. 1, pp. 568–587

KINETIC CHEMOTAXIS TUMBLING KERNEL DETERMINED FROM MACROSCOPIC QUANTITIES*

KATHRIN HELLMUTH†, CHRISTIAN KLINGENBERG†, QIN LI‡, AND MIN TANG§

Abstract. Chemotaxis is the physical phenomenon that bacteria adjust their motions according to chemical stimulus. A classical model for this phenomenon is a kinetic equation that describes the velocity jump process whose tumbling/transition kernel uniquely determines the effect of a chemical stimulus on bacteria. The model has been shown to be an accurate model that matches with bacteria motion qualitatively. For a quantitative modeling, biophysicists and practitioners are also highly interested in determining the explicit value of the tumbling kernel. Due to the experimental limitations, measurements are typically macroscopic in nature. Do macroscopic quantities contain enough information to recover microscopic behavior? In this paper, we give a positive answer. We show that when given a special design of initial data, the population density, one specific macroscopic quantity as a function of time, contains sufficient information to recover the tumbling kernel and its associated damping coefficient. Moreover, we can read off the chemotaxis tumbling kernel using the values of population density directly from this specific experimental design. This theoretical result using kinetic theory sheds light on how practitioners may conduct experiments in laboratories.

Key words. kinetic chemotaxis equation, velocity jump process, singular decomposition, unique reconstruction, tumbling kernel

MSC codes. 92C17, 35R30, 35Q92, 35R09, 45K05

DOI. 10.1137/22M1499911

1. Introduction.

Bacteria and microorganisms can move autonomously and react to external stimuli, such as food or danger, which is an important factor in evolution. If the movement is affected by a chemical stimulus, this phenomenon is called chemotaxis. Chemotaxis phenomena are widely observed among motile organisms and particularly well studied for Escherichia coli (E.coli) cells. When the bacterial movement consists of two alternating phases in which they either run along a straight line or reorient by changing the direction of travel (tumbling), their movement is called a velocity jump process.

The kinetic chemotaxis model describes this behavior statistically [1, 9, 15, 30]:

$$\frac{\partial}{\partial t} f(x,t,v) + v \cdot \nabla_x f(x,t,v) = \mathcal{L}(f)(x,t,v) - \sigma(x,v) f(x,t,v), \tag{1.1}$$

$$f(x,t=0,v) = \phi(x,v). \tag{1.2}$$

*Received by the editors June 1, 2022; accepted for publication (in revised form) September 6, 2023; published electronically January 10, 2024.
https://doi.org/10.1137/22M1499911
Funding: The first author acknowledges support by the *Würzburg Mathematics Center for Communication and Interaction* (WMCCI) as well as the *German Academic Scholarship Foundation* (Studienstiftung des deutschen Volkes) and the *Marianne-Plehn-Program.* The work of the third author is supported in part by NSF-DMS-1750488 and ONR-N00014-21-1-2140, and the Vilas Young Investigator award. The fourth author is supported by NSFC 11871340, NSFC12031013.

†Department of Mathematics, University of Würzburg, Würzburg, 97074, Germany (kathrin.hellmuth@uni-wuerzburg.de, https://www.mathematik.uni-wuerzburg.de/en/fluidmechanics/team/kathrin-hellmuth/; klingen@mathematik.uni-wuerzburg.de, https://www.mathematik.uni-wuerzburg.de/en/fluidmechanics/team/christian-klingenberg/).

‡Department of Mathematics, University of Wisconsin-Madison, Madison, WI 53705 USA (qinli@math.wisc.edu, https://math.wisc.edu/staff/li-qin/).

§School of Mathematics, Shanghai Jiao Tong University, Shanghai, 200240, China (tangmin@sjtu.edu.cn, https://ins.sjtu.edu.cn/people/mtang/).

The equation describes the evolution of the population density of bacteria $f(x,t,v)$ on the phase space $(x,v) \in \mathbb{R}^d \times V$, $d \in \{2,3\}$, during the time interval $t \in [0,T]$ with initial condition ϕ. Experimental data suggest that bacteria move at a constant speed, and we set $V := \mathbb{S}^{d-1}$ to reflect this fact.

The left side of (1.1) describes the motion of the bacteria moving along a straight line in direction v from location x. The two terms $\mathcal{L}(f)$ and σf on the right-hand side of the equation describe the velocity jump process arising from the reorientation by tumbling. In particular,

$$\mathcal{L}(f)(x,t,v) = \int_V K(x,v,v')f(x,t,v')\mathrm{d}v' \tag{1.3}$$

collects the particles that change their velocity from v' to v, and

$$\sigma(x,v) = \int_V K(x,v',v)\mathrm{d}v' \tag{1.4}$$

describes the fraction of particles changing velocity from v to others, and thus disappearing in a statistical sense from the phase point (x,t,v). As such, these two terms are called the gain and loss terms, respectively. We should note that in real applications, bacteria sometimes generate self-attraction/propulsion and this self-generated stimulus should be included in the tumbling kernel $K(x,v,v')$ through the "concentration" term; see chemotaxis modeling [7, 8, 9, 10]. In our paper we assume this is the next order concern, and set K to be a fixed function in space. Then our model turns to be a linear Boltzmann equation. We discuss more details in the conclusion section 5.

Different types of bacteria take different values of K and σ and are differently affected by the concentrations of the chemical stimulus (chemoattractant). Since the tumbling kernel K and the damping factor σ uniquely determine the law of the bacterial motion in (1.1), biologists and practitioners are highly interested in identifying them for future motion predictions; see important applications in bioreactors [37], the spread and prevention of diseases [20], and biofilm formation [28].

To identify K and σ in practice, experiments are conducted to measure observables of bacterial behavior so to indirectly infer the tumbling coefficient. The practical difficulty is that measuring the time dynamical data of velocity dependent bacteria density $f(x,t,v)$ is not always feasible. One would have to trace the trajectory of each single bacterium for a long time, which is technically difficult when there are a lot of bacteria [19]. Instead, the time evolution of the macroscopic quantities such as the density,

$$\rho(x,t) := \langle f \rangle = \int_V f \,\mathrm{d}v,$$

is much easier to obtain by counting bacteria on a time series of photos; see also other more sophisticated methods [21]. This poses an interesting mathematical question: can the macroscopic measurements on bacteria density, as a function of time, uniquely determine the values of K and σ?

At first sight, the answer should be negative. Indeed, the to-be-inferred parameters are functions posed on the microscopic level and have v dependence, while the measurements are purely on the macroscopic level with v dependence eliminated. This mismatch leads to some mathematical difficulty, to overcome which, a mechanism that triggers information on the microscopic level is needed. We introduce this

mechanism by examining the time dependence, and playing with the singularity in the initial data. It turns out that if one places a special set of singularity in the initial data and introduces the corresponding singularity to the measuring operator that is concentrated at the compatible time and location, we can prove that the coefficients K and σ are uniquely reconstructable. Furthermore, the values can be directly read off from the measurements.

The mathematical machinery that allows us to explicitly express the reconstruction is a technique termed singular decomposition. It is a technique that is specifically designed for studying inverse problems from kinetic theory, and has been traditionally used to investigate stationary radiative or photon transport equation; see [2, 3, 4, 6, 12, 24, 33, 38] for instance. The most classical use of the singular decomposition allows the data to be v dependent, but the measuring location is typically set only to be on the boundary. Difficulties are introduced when only velocity independent measurements are available [5, 11, 33, 44]. In this setting, one no longer has the luxury of freedom from the velocity dependence. In our project, however, we use measurements in time, containing information from the interior of the domain. The main task in this project is to investigate if this freedom could counter the difficulties induced by the loss of velocity information. It turns out from our study that the availability of short time data is also crucial. In both the reconstruction of σ and K, we heavily rely on the design of initial/measuring time and locations that precisely reflect the parameters to be reconstructed.

Using measurements to identify bacteria motion is of high practical interests to biologists. However, even though chemotaxis and inverse problems are both very active areas of research, largely hindered by the lack of rigorous mathematical tools, very little is known theoretically if the experiments can truly reflect bacteria chemotaxis behavior. In practice, the most popular parabolic Keller–Segel model is on the macroscopic level, and it is common for practitioners to assume a heuristically obtained parametrized form for the model coefficients and estimate only these parameters by experimental data [18, 17, 34, 40]. Numerically, one can study the identifiability of the chemoattractant sensitivity for the macroscopic models, as in [14, 16], where it was shown how the reconstruction from the regularized problem converges to the true solution as the noise vanishes.

As the techniques such as kinetic theory and singular decomposition ripen, we are convinced that these applications can be reexamined afresh, with a more rigorous viewpoint. It is our aim to prove the unique reconstructability of the kinetic tumbling kernel K and loss coefficient σ using only the macroscopic measurements. Hopefully these arguments provide foundations to the algorithms that execute the reconstruction in reality.

The article is structured as follows: In section 2, we provide the problem setup. Sections 3 and 4 build the heart of this article and contain the proofs of the unique reconstructability of σ and K, respectively. For both cases, the singular decomposition technique will be used for carefully prepared initial data and measurement test function. The article is concluded by section 5.

2. Problem setup. We describe the setup of the lab experiment in this section.

In the lab experiment, bacteria are placed in an environment with a fixed chemical concentration in a controlled manner, so K and σ can be thought as constants in time. Along time, we take measurement of the macroscopic bacteria density locally in time and space.

Mathematically we view (1.1) as the model equation for bacteria motion. Though bacteria are supported in an agar plate so the plate provides certain boundary con-

ditions, for simplicity, we assume the domain is infinitely big so the boundary has no effect on the dynamics. We should note, however, that the inversion mechanism that is to be employed in this paper requires a compactly supported initial condition and data measurement at small time, so boundary conditions, even if included in the system, are expected to play no role in the reconstruction. Hence we expect the inversion mechanism to be easily extended to treat the interior of a finite domain problem in a rather straightforward manner.

The initial condition can be controlled, and we prescribe it as $\phi(x,v)$. In particular, singularity in the v domain can be realized. To be more specific, in lab experiments, one can confine bacteria in a thin pipe and release bacteria from the pipe into the environment to generate an initial condition that is singular in velocity. These experiments were conducted, for example, in [39] where E.coli bacteria were examined, and in [26] where the authors manipulated synthetic microswimmers through microconfinement. The authors of [43] and the references therein investigate another possibility, showing that Euglena gracilis algae can be controlled by polarized light.

All results in this paper are presented for $d=3$, but the method can be extended to deal with a $d=2$-dimensional setup as well.

For all given initial data $\phi(x,v)$, we denote the solution to the PDE (1.1) equipped with initial data (1.2) by f_ϕ, and the macroscopic quantity is

$$\rho_\phi(x,t) := \langle f_\phi \rangle = \int_V f_\phi \,\mathrm{d}v\,.$$

This builds the following map:

$$\Lambda_K : \phi \quad \to \quad \rho_\phi(t,x)\,.$$

To be more compatible with the real practice, for each detector, we let $\psi(x,t) \in C_c^\infty$ present its profile, then the detector's reading would be ρ_ϕ tested on this test function, the output of the following measurement operator:

$$M_\psi(f_\phi) = M_\psi(\rho_\phi) = \int_0^T \int_{\mathbb{R}^3} \rho_\phi\, \psi(x,t)\,\mathrm{d}x\,\mathrm{d}t\,. \tag{2.1}$$

Since the measurement operator only acts on the density ρ_ϕ, we abuse the notation and let $M_\psi(f_\phi) = M_\psi(\rho_\phi)$ when $\rho_\phi = \langle f_\phi \rangle$.

It is immediate that for every fixed ψ, the measurement is the one instance of reading of $\Lambda_K[\phi]$:

$$M_\psi(f_\phi) = \int_0^T \int_{\mathbb{R}^3} \psi(t,x)\Lambda_K[\phi](t,x)\,\mathrm{d}t\,\mathrm{d}x\,.$$

We claim that Λ_K encodes all the needed information to uniquely recover σ and K, and the reconstruction process depends on the special design of ϕ and ψ, namely, the following.

THEOREM 2.1. *Under mild conditions, one can uniquely reconstruct σ and K using the map Λ_K. Moreover, by properly choosing (ϕ,ψ), the reconstruction can be explicit using the reading of $M_\psi(f_\phi)$.*

Throughout the paper we assume σ and K are time independent, and the admissible sets are,

$$\mathcal{A}_\sigma = \{\sigma \in C_+(\mathbb{R}^3 \times V) \mid \|\sigma\|_\infty \le C_\sigma\},$$
$$\mathcal{A}_K = \{K \in C_+(\mathbb{R}^3 \times W) \mid \|K\|_\infty \le C_K\},$$

where we set $W := \{(v, v') \in V \times V \mid v \neq v'\}$. The reconstruction procedure is performed on these sets.

3. Reconstructing σ. We dedicate this section to reconstructing $\sigma(x, v)$, and showing the following theorem.

THEOREM 3.1 (unique reconstruction of σ). *Let $\sigma \in \mathcal{A}_\sigma$ and $K \in \mathcal{A}_K$. The map Λ_K uniquely determines $\sigma(x, v)$. In particular, for any (x, v), by a proper choice of ϕ and ψ, one can explicitly express $\sigma(x, v)$ in terms of $M_\psi(\rho_\phi)$, with ρ_ϕ being the density associated with f_ϕ that solves* (1.1).

Remark 3.2. We note the statement of the result can be extended to treat time dependent σ as well. To recover $\sigma(x, t, v)$ at a particular time t-horizon, the data ϕ need to be provided, and the measurements need to be collected close enough to t. As the following proof shows, if ϕ is provided at $t_0 > t - C$ with $C = (|V|C_K)^{-1}$ for C_K being the bound from the admissible set, the time dependence of σ can be reconstructed as well.

The main technique used in the proof is termed the singular decomposition developed in [12], and then extensively used in other following works [2, 3, 4, 6, 24, 38]. The idea is to design a special set of sources ϕ that introduces singularity to the solution. In a short time, the singularity is mostly preserved along the propagation trajectory. By properly choosing the compatible ψ, the singular information can be picked up by the measurements. Mathematically, to identify the singular component of the solution, we decompose f_ϕ into parts that exhibit different regularity. In particular, we decompose f into

$$f_\phi = f_{\phi,0} + f_{\phi,\geq 1},$$

where $f_{\phi,0}$ and $f_{\phi,\geq 1}$ solve the following equations, respectively:

$$\begin{cases} \partial_t f_{\phi,0} + v \cdot \nabla f_{\phi,0} &= -\sigma f_{\phi,0}, \\ f_{\phi,0}(x, t = 0, v) &= \phi(x, v), \end{cases} \tag{3.1}$$

and

$$\begin{cases} \partial_t f_{\phi,\geq 1} + v \cdot \nabla f_{\phi,\geq 1} &= -\sigma f_{\phi,\geq 1} + \mathcal{L}(f_{\phi,0} + f_{\phi,\geq 1}), \\ f_{\phi,\geq 1}(x, t = 0, v) &= 0. \end{cases} \tag{3.2}$$

As a direct consequence,

$$M_\psi(\rho_\phi) = M_\psi(\rho_{\phi,0}) + M_\psi(\rho_{\phi,\geq 1}),$$

where we denote $\rho_{\phi,i} := \int f_{\phi,i} \mathrm{d}v \quad \text{for} \quad i \in \{0, \geq 1\}$.

Intuitively, the division of f_ϕ into the two components is to separate the particles that behave differently. In particular, $f_{\phi,0}$ denotes the number of bacteria on the phase space that tumble out of the state they were in. So in some sense, the distribution function "decays" along the trajectory with rate σ. $f_{\phi,\geq 1}$, on the other hand, collects the distribution of all remaining bacteria. The right-hand side of (3.2) has three terms, representing the bacteria tumbling out of the state (thereby decaying in the distribution sense by σ), tumbling in from the source $f_{\phi,0}$, and tumbling in by $f_{\phi,\geq 1}$. Since $f_{\phi,0}$ contains σ information solely, one would expect to reconstruct σ if $f_{\phi,0}$ information can be identified from the full f_ϕ.

The core of analysis lies in designing a special set of ϕ and ψ that has compatible singularities to each other so that

$$M_\psi(\rho_\phi) = M_\psi(\rho_{\phi,0}) \quad \text{and} \quad M_\psi(\rho_{\phi,\geq 1}) = 0\,, \tag{3.3}$$

so we have access to the value of $M_\psi(\rho_{\phi,0})$ that will be further used to reconstruct σ. When the context is clear below, we drop the ϕ dependence in ρ to have a concise notation.

We now list the conditions for ϕ and ψ so to have (3.3) hold true. Let $\phi_x, \psi_x \in C_c^\infty(\mathbb{R}^3)$, $\phi_v \in C_c^\infty(\mathbb{R}^2)$, and $\psi_t \in C_c^\infty(\mathbb{R})$ be nonnegative functions compactly supported in the unit ball $B^n(0,1) \subset \mathbb{R}^n$:

$$\begin{aligned} &\operatorname{supp}(\phi_x), \operatorname{supp}(\psi_x) \subset B^3(0,1), \quad \operatorname{supp}(\phi_v) \subset B^2(0,1), \quad \operatorname{supp}(\psi_t) \subset B^1(0,1), \\ &0 \le \phi_x, \psi_x, \phi_v, \psi_t \le 1 \quad \text{with} \quad \phi_x(0) = \psi_x(0) = \phi_v(0) = \psi_t(0) = 1, \quad \text{and} \\ &1 = \int_{\mathbb{R}^3} \phi_x(x)\,\mathrm{d}x = \int_{\mathbb{R}^3} \psi_x(x)\,\mathrm{d}x = \int_{\mathbb{R}^2} \phi_v(y)\,\mathrm{d}y = \int_{\mathbb{R}} \psi_t(t)\,\mathrm{d}t. \end{aligned} \tag{3.4}$$

Letting $(x_i, v_i) \in \mathbb{R}^3 \times V$ be the initial location and velocity of the bacteria concentration, and $(x_m, t_m) \in \mathbb{R}^3 \times (0,T)$ be the measurement location and time, we now set the initial data ϕ and measurement test function ψ to be

$$\begin{aligned} \phi(x,v) &= \frac{1}{\varepsilon^3\delta^2}\phi_x\left(\frac{x-x_i}{\varepsilon}\right)\phi_v\left(\frac{\mathbb{P}_{v_i}(v)}{\delta}\right) j(v;v_i) && \in C_c^\infty, \\ \psi(x,t) &= \frac{1}{\eta}\psi_x\left(\frac{x-x_m}{\varepsilon}\right)\psi_t\left(\frac{t-t_m}{\eta}\right) && \in C_c^\infty \end{aligned} \tag{3.5}$$

for small scaling parameters $\varepsilon, \delta, \eta > 0$. Furthermore, $\mathbb{P}_{v_i} : \mathbb{S} \setminus \{-v_i\} \to \mathbb{R}^2$ denotes the stereographic projection on the direction of $-v_i$, with its absolute Jacobi determinant given by $j(v;v_i) := 1/((1+\langle v, v_i\rangle)^2 |\langle v, v_i\rangle|)$. Accordingly, we also define a quantity that will be used in the later discussion:

$$C_{\phi,\psi} = \int_{\mathbb{R}^3} \phi_x(x)\,\psi_x(x)\,\mathrm{d}x\,. \tag{3.6}$$

For the measurement $M_\psi(\rho_{\phi,0})$ to be nontrivial, the two pairs (x_i, v_i) and (x_m, t_m) should be compatible to each other. Indeed, we require

$$x_m := x_m(t_m) = x_i + v_i t_m\,,$$

so that the measurement location at t_m indeed receives the data transported from x_i in the direction of v_i.

The proof of the theorem is based on the following two lemmas.

LEMMA 3.3. *Let ϕ and ψ be defined as in* (3.5). *Let σ and K be selected from the admissible sets. The solution to* (3.1) *gives*

$$\lim_{\varepsilon\to 0}\lim_{\eta,\delta\to 0} M_\psi(\rho_0) = e^{-\int_0^{t_m}\sigma(x_i+v_i s, v_i)\,\mathrm{d}s} C_{\phi_x\psi_x}\,.$$

Similarly, we have the following lemma.

LEMMA 3.4. *Let ϕ and ψ be defined as in* (3.5), *with $t_m < T$ that satisfies $C_K|V|T < 1$. Let σ and K be selected from the admissible sets. The solution to* (3.2) *gives*

$$\lim_{\varepsilon\to 0}\lim_{\delta,\eta\to 0} M_\psi(\rho_{\ge 1}) = 0\,.$$

Theorem 3.1 is a quick corollary of these two lemmas.

Proof of Theorem 3.1. Under the conditions listed in Lemmas 3.3 and 3.4, we have

$$\lim_{\varepsilon\to 0}\lim_{\eta,\delta\to 0} M_\psi(\rho_\phi) = \lim_{\varepsilon\to 0}\lim_{\eta,\delta\to 0} M_\psi(\rho_0) = C_{\phi_x\psi_x} e^{-\int_0^{t_m}\sigma(x_i+v_i s, v_i)\,\mathrm{d}s}\,.$$

Then we have the immediate conclusion that

$$\sigma(x_m, v_i) = -\partial_{t_m} \ln\left(\frac{1}{C_{\phi_x\psi_x}} \lim_{\varepsilon\to 0} \lim_{\delta,\eta\to 0} (M_\psi(\rho_\phi))\right). \tag{3.7}$$

∎

Remark 3.5. We stress that the result only provides a unique reconstruction but does not give a stability bound. The explicit reconstruction of σ is seen in (3.7). However, we should note that the formula includes a time derivative outside the limit taking of the small parameters. This may bring some extra difficulty in the stability analysis. Moreover, we would like to point out that both lemmas and the proof of the theorem do not have specific dimension dependence. The result holds true for $d = 2$ as well. This is slightly different from the classical kinetic inverse problem using an albedo operator to infer photon scattering coefficient. Since in these problems, the data are confined on the boundary, so the data automatically lose one dimension of freedom, making the results sensitive to the dimensionality of the problem. Here the data are taken in the interior and we have the freedom to adjust time. This mechanism is independent of the dimension d so the result easily extends.

We now give proofs for the two lemmas above. It amounts to detailed calculations.

Proof of Lemma 3.3. According to the equation for f_0 in (3.1), we can explicitly compute f_0 along the trajectory of the bacteria propagation:

$$f_0(x,t,v) = e^{-\int_0^t \sigma(x-vs,v)\,\mathrm{d}s}\phi(x-vt,v)\,. \tag{3.8}$$

Inserting this into the definition of the measurement (2.1), we have

$$\begin{aligned} M_\psi(\rho_0) &= \int_0^T \int_{\mathbb{R}^3} \int_V f_0(x,t,v)\,\mathrm{d}v\,\psi(x,v)\,\mathrm{d}x\,\mathrm{d}t \\ &= \int_0^T \int_{\mathbb{R}^3} \int_V e^{-\int_0^t \sigma(x-vs,v)\,\mathrm{d}s}\phi(x-vt,v)\,\mathrm{d}v\,\psi(x,t)\,\mathrm{d}x\,\mathrm{d}t\,. \end{aligned}$$

Plugging the form of ϕ and ψ into (3.5), we have

$$\begin{aligned} &M_\psi(\rho_0) \\ &= \frac{1}{\varepsilon^3\delta^2\eta}\int_0^T \int_{\mathbb{R}^3}\int_V e^{-\int_0^t \sigma(x-vs,v)\,\mathrm{d}s}\phi_x\left(\frac{x-vt-x_i}{\varepsilon}\right)\phi_v\left(\frac{\mathbb{P}_{v_i}(v)}{\delta}\right) j(v)\,\mathrm{d}v \\ &\qquad \cdot \psi_x\left(\frac{x-x_m}{\varepsilon}\right)\psi_t\left(\frac{t-t_m}{\eta}\right)\mathrm{d}x\,\mathrm{d}t \\ &= \frac{1}{\varepsilon^3}\int_{-\frac{t_m}{\eta}}^{\frac{T-t_m}{\eta}} \int_{\mathbb{R}^3}\int_{\mathbb{R}^2} e^{-\int_0^{t_m+\eta\tilde{t}} \sigma(x-\mathbb{P}_{v_i}^{-1}(\delta y)s,\mathbb{P}_{v_i}^{-1}(\delta y))\,\mathrm{d}s}\ \phi_x\left(\frac{x-\mathbb{P}_{v_i}^{-1}(\delta y)(t_m+\eta\tilde{t})-x_i}{\varepsilon}\right) \\ &\qquad \cdot \phi_v(y)\,\psi_x\left(\frac{x-x_m}{\varepsilon}\right)\psi_t\left(\tilde{t}\right)\,\mathrm{d}y\,\mathrm{d}x\,\mathrm{d}\tilde{t}, \end{aligned}$$

where we substituted $\tilde{t} := \frac{t-t_m}{\eta}$ and $y := \frac{\mathbb{P}_{v_i}(v)}{\delta}$ into the last equation. Now fixing ε and letting $\eta \to 0$, $\delta \to 0$, then by continuity of σ,ϕ_x, $\mathbb{P}_{v_i}^{-1}$, and (3.4), the dominated convergence theorem yields

$$\begin{aligned}
&\lim_{\eta,\delta\to 0} M_\psi(\rho_0)\\
&\quad = \frac{1}{\varepsilon^3}\int_{\mathbb{R}^3} e^{-\int_0^{t_m}\sigma(x-v_i s,v_i)\,\mathrm{d}s}\phi_x\left(\frac{x-v_i t_m-x_i}{\varepsilon}\right)\psi_x\left(\frac{x-x_m}{\varepsilon}\right)\mathrm{d}x\\
&\qquad\cdot\int_{\mathbb{R}}\psi_t\left(\tilde{t}\right)\mathrm{d}\tilde{t}\int_{\mathbb{R}^2}\phi_v\left(y\right)\mathrm{d}y\\
&\quad = \int_{\mathbb{R}^3} e^{-\int_0^{t_m}\sigma(x_m+\varepsilon\tilde{x}-v_i s,v_i)\,\mathrm{d}s}\phi_x\left(\tilde{x}\right)\psi_x\left(\tilde{x}\right)\mathrm{d}\tilde{x}\,.
\end{aligned}$$

We used the substitution $\tilde{x} := \frac{x-x_m}{\varepsilon}$ in the last equation. Now set $\epsilon \to 0$ and using the continuity of σ, we obtain

$$\begin{aligned}
&\lim_{\varepsilon\to 0}\lim_{\eta,\delta\to 0} M_\psi(f_{\phi,0})\\
&\quad = e^{-\int_0^{t_m}\sigma(x_m-v_i s,v_i)\,\mathrm{d}s}\int_{\mathbb{R}^3}\phi_x\left(\tilde{x}\right)\psi_x\left(\tilde{x}\right)\mathrm{d}\tilde{x} = e^{-\int_0^{t_m}\sigma(x_i+v_i s,v_i)\,\mathrm{d}s}C_{\phi_x\psi_x}\,,
\end{aligned}$$

where we used (3.6). The proof is concluded. ∎

To prove Lemma 3.4, we will first introduce the following lemma.

LEMMA 3.6. *Let g satisfy the following equation,*

$$\begin{cases}\partial_t g + v\cdot\nabla g = -\sigma g + \mathcal{L}(g) + \mathcal{L}(h)\,, \quad (x,t,v)\in\mathbb{R}^3\times[0,T]\times V,\\ g(x,t=0,v) = 0\,,\end{cases} \tag{3.9}$$

where $\mathcal{L}$ and σ are defined in (1.3)–(1.4) *for $K\in\mathcal{A}_K$ and h is a given positive function, then the measurement of g with respect to a general measurement test function $\psi\in C_c^\infty$ is bounded by*

$$M_\psi(\langle g\rangle) \le C_K|V|e^{C_K|V|T}M_\psi\left(\int_0^t \operatorname*{ess\,sup}_x(\langle h\rangle(x,s))\,\mathrm{d}s\right). \tag{3.10}$$

Proof. The proof is a direct calculation. Integrating (3.9) along the characteristics, we have

$$\begin{aligned}
\operatorname*{ess\,sup}_x\langle g\rangle &= \operatorname*{ess\,sup}_x\int_V g(x,t,v)\,\mathrm{d}v\\
&= \operatorname*{ess\,sup}_x\int_V\int_0^t\left[-\sigma g+\mathcal{L}(g)+\mathcal{L}(h)\right](x-vs,t-s,v)\,\mathrm{d}s\,\mathrm{d}v\\
&\le C_K\int_V\int_0^t(\operatorname*{ess\,sup}_x\langle g\rangle+\operatorname*{ess\,sup}_x\langle h\rangle)(x-vs,t-s))\,\mathrm{d}s\,\mathrm{d}v\\
&= C_K|V|\int_0^t\operatorname*{ess\,sup}_x(\langle g\rangle(x,s))\,\mathrm{d}s+\underbrace{C_K|V|\int_0^t\operatorname*{ess\,sup}_x(\langle h\rangle(x,s))\,\mathrm{d}s}_{=:\alpha(t)},
\end{aligned}$$

where we used the positivity of g [27] and σ as well as the boundedness of K in the inequality and a change of variables. We call the integral form of Gronwall's lemma and use the fact that $g(x,t=0,v)=0$ and α is nondecreasing in order to obtain

$$\operatorname*{ess\,sup}_x \langle g\rangle \le \alpha(t) e^{\int_0^t C_K|V|\mathrm{d}s} = C_K|V| e^{C_K|V|t} \int_0^t \operatorname*{ess\,sup}_x (\langle h\rangle(x,s))\,\mathrm{d}s.$$

Noting that $M_\psi(\langle g\rangle)$ is a linear operator and preserves the monotonicity, we conclude (3.10). ∎

With the above lemma at hand, we can readily prove Lemma 3.4.

Proof of Lemma 3.4. We further decompose $f_{\ge 1} = f_1 + f_2 + \cdots + f_N + f_{\ge N+1}$ for some $N \in \mathbb{N}$ to be chosen later, with each level of f_n, $n \ge 1$, satisfying

$$\begin{cases} \partial_t f_n + v\cdot\nabla f_n = -\sigma f_n + \mathcal{L}(f_{n-1}), \\ f_n(x, t=0, v) = 0, \end{cases} \tag{3.11}$$

and the last level

$$\begin{cases} \partial_t f_{\ge N+1} + v\cdot\nabla f_{\ge N+1} = -\sigma f_{\ge N+1} + \mathcal{L}(f_N) + \mathcal{L}(f_{\ge N+1}), \\ f_{\ge N+1}(x, t=0, v) = 0. \end{cases}$$

Then the measurement decomposes accordingly, i.e.,

$$M(\rho_{\ge 1}) = M(\rho_1) + M(\rho_2) + \cdots + M(\rho_N) + M(\rho_{\ge N+1}).$$

Our objective is to show that in the scaling limit, all the $M(\rho_i)$ vanish for $i \le N$ and $M(\rho_{\ge N+1})$ is arbitrarily small for a big N.

- To do so we first write an explicit expression for $M(\rho_n)$ for an arbitrary $n \in \mathbb{N}$. We integrate (3.11) along characteristics and use the fact that σ, f_n are nonnegative to see that

$$\begin{aligned} f_n(x,t,v_0) &= \int_0^t [-\sigma f_n + \mathcal{L}(f_{n-1})](x - v_0 s_0, t - s_0, v_0)\,\mathrm{d}s_0 \\ &\le C_K \int_0^t \langle f_{n-1}\rangle (x - v_0 s_0, t - s_0)\,\mathrm{d}s_0 \\ &= C_K \int_0^t \int_V f_{n-1}(x - v_0 s_0, t - s_0, v_1)\,\mathrm{d}v_1\,\mathrm{d}s_0. \end{aligned}$$

  In this notation, v_0 is the last direction in which the bacteria of f_n run, and s_0 is the time for which they run into this direction. Respectively, v_j, and s_j denote the direction and time in which the bacteria run after their $(n-j)$-th tumble.
  By induction,

(3.12)
$$\begin{aligned} &f_n(x,t,v_0) \\ &\le C_K^n \int_0^t \int_V \int_0^{t-s_0} \int_V \cdots \int_0^{t-\sum_{j=0}^{n-2} s_j} \int_V f_0\left(x - \sum_{j=0}^{n-1} s_j v_j, t - \sum_{j=0}^{n-1} s_j, v_n\right) \\ &\qquad \mathrm{d}v_n\,\mathrm{d}s_{n-1}\ldots\mathrm{d}v_2\,\mathrm{d}s_1\,\mathrm{d}v_1\,\mathrm{d}s_0 \\ &\le C_K^n \int_0^t \int_V \cdots \int_0^{t-\sum_{j=0}^{n-2} s_j} \int_V \phi\left(x - \sum_{j=0}^{n-1} s_j v_j - \left(t - \sum_{j=0}^{n-1} s_j\right) v_n, v_n\right) \\ &\qquad \mathrm{d}v_n\,\mathrm{d}s_{n-1}\ldots\mathrm{d}v_1\,\mathrm{d}s_0, \end{aligned}$$

where we bounded $f_0(x,t,v)$ by $\phi(x-vt,v)$ using (3.8) and noting $\sigma \geq 0$. Inserting this into the measurement and calling the dominated convergence theorem, we have

$$
\begin{aligned}
&M(\rho_n)\\
&\quad= \int_{\mathbb{R}^3}\int_0^T\int_V f_n(x,t,v_0)\,\mathrm{d}v_0\,\psi(x,t)\,\mathrm{d}t\,\mathrm{d}x\\
&\quad\leq C_K^n \int_{\mathbb{R}^3}\int_0^T\int_V \left[\int_0^t\int_V\cdots\int_0^{t-\sum_{j=0}^{n-2}s_j}\int_V \phi\left(x-\sum_{j=0}^{n-1}s_jv_j\right.\right.\\
&\qquad\left.\left.-\left(t-\sum_{j=0}^{n-1}s_j\right)v_n, v_n\right)\mathrm{d}v_n\,\mathrm{d}s_{n-1}\ldots\mathrm{d}v_1\,\mathrm{d}s_0\right]\mathrm{d}v_0\,\psi(x,t)\,\mathrm{d}t\,\mathrm{d}x\\
&\quad\xrightarrow{\delta,\eta\to 0} C_K^n \int_{\mathbb{R}^3}\int_V\int_0^{t_m}\int_V\cdots\int_0^{t_m-\sum_{j=0}^{n-2}s_j}\frac{1}{\varepsilon^3}\psi_x\left(\frac{x-x_m}{\varepsilon}\right)\\
&\qquad\qquad\cdot\phi_x\left(\frac{x-\sum_{j=0}^{n-1}s_jv_j-\left(t_m-\sum_{j=0}^{n-1}s_j\right)v_i-x_i}{\varepsilon}\right)\\
&\qquad\qquad\mathrm{d}s_{n-1}\ldots\mathrm{d}v_1\,\mathrm{d}s_0\,\mathrm{d}v_0\,\mathrm{d}x\\
&\quad= C_K^n \int_{\mathbb{R}^3}\int_V\int_0^{t_m}\int_V\cdots\int_0^{t_m-\sum_{j=0}^{n-2}s_j}\psi_x(\tilde{x})\\
&\qquad\qquad\cdot\phi_x\left(\tilde{x}+\frac{\sum_{j=0}^{n-1}s_j(v_i-v_j)}{\varepsilon}\right)\mathrm{d}s_{n-1}\ldots\mathrm{d}v_1\,\mathrm{d}s_0\,\mathrm{d}v_0\,\mathrm{d}\tilde{x}.
\end{aligned}
$$

In the last line we used the substitution $\tilde{x}=\frac{x-x_m}{\varepsilon}=\frac{x-x_i-v_it_m}{\varepsilon}$. Now for $\varepsilon\to 0$, one has

$$
\phi_x\left(\tilde{x}+\frac{\sum_{j=0}^{n-1}s_j(v_i-v_j)}{\varepsilon}\right)\to\phi(\tilde{x})\mathbb{1}_0\left(\sum_{j=0}^{n-1}s_j(v_i-v_j))\right),
$$

where $\mathbb{1}$ denotes the indicator function.[1] Using the dominated convergence theorem again, we have

$$
\begin{aligned}
\lim_{\varepsilon\to 0}\lim_{\delta,\eta\to 0} M(\rho_n) &\leq C_{\phi,\psi}C_K^n\int_V\int_0^{t_m}\int_V\cdots\int_0^{t_m-\sum_{j=0}^{n-2}s_j}\mathbb{1}_0\left(\sum_{j=0}^{n-1}s_j(v_i-v_j)\right)\\
&\qquad\qquad\mathrm{d}s_{n-1}\ldots\mathrm{d}v_1\,\mathrm{d}s_0\,\mathrm{d}v_0\\
&= 0,
\end{aligned}
$$

where the last equality holds true, because the integration is taken on a measure-zero set for a bounded integrand. We conclude $M_\psi(\rho_n)=0$ in the limit of $\epsilon,\delta,\eta\to 0$.

[1] $\mathbb{1}_A(a)=1$ for a is in the set A and zero elsewhere and $\mathbb{1}_{a'}:=\mathbb{1}_{\{a'\}}$ for elements a' in some set.

- We now proceed to show the smallness of $M(\rho_{\geq N+1})$. Applying Lemma 3.6 with $g := f_{\geq N+1}, h := f_N$, we have

$$M(\rho_{\geq N+1}) \leq C_K|V|e^{C_K|V|T} M\left(\int_0^t \operatorname*{ess\,sup}_x \langle f_N\rangle(x,s)\,\mathrm{d}s\right). \tag{3.13}$$

Using estimate (3.12) for f_N as well as $\max_x \phi(x,v) \leq \frac{1}{\varepsilon^3\delta^2}\phi_v\left(\frac{\mathbb{P}_{v_i}(v)}{\delta}\right) j(v;v_i)$, we have

$$\begin{aligned}
&\int_0^t \operatorname*{ess\,sup}_x \langle f_N\rangle(x,s)\,\mathrm{d}s \\
&\leq C_K^N \int_0^t \int_V \Big[\int_0^s \int_V \cdots \int_0^{s-\sum_{j=0}^{N-2} s_j} \int_V \frac{1}{\varepsilon^3\delta^2}\phi_v\left(\frac{\mathbb{P}_{v_i}(v_N)}{\delta}\right) j(v_N;v_i) \\
&\qquad\qquad \mathrm{d}v_N\,\mathrm{d}s_{N-1}\ldots\mathrm{d}v_1\,\mathrm{d}s_0\Big]\,\mathrm{d}v_0\,\mathrm{d}s \\
&\leq \frac{1}{\varepsilon^3} C_K^N |V|^N t^{N+1} \int_V \frac{1}{\delta^2}\phi_v\left(\frac{\mathbb{P}_{v_i}(v_N)}{\delta}\right) j(v_N;v_i)\,\mathrm{d}v_N.
\end{aligned}$$

Since the above integral over v_N has value 1, (3.13) gives

$$\begin{aligned}
M(\rho_{\geq N+1}) &\leq (C_K|V|T)^{N+1} e^{C_K|V|T} \int_{\mathbb{R}^3}\int_0^T \frac{1}{\varepsilon^3}\psi(x,t)\,\mathrm{d}t\,\mathrm{d}x \\
&\leq (C_K|V|T)^{N+1} e^{C_K|V|T}.
\end{aligned}$$

This shows $M(\rho_{\geq N+1})$ becomes arbitrarily small as N grows, when $C_K|V|T < 1$. In summary, this proves Lemma 3.4. ∎

4. Reconstructing K. This section is dedicated to the reconstruction of K from macroscopic measurements of the bacteria density ρ. The idea is similar to the previous section: A class of special functions are used as the initial conditions and the measurement test functions are designed accordingly. These functions carry a certain type of singularity and are designed to be compatible with each other, so the measurement singles out a trajectory that we would like to get information about. In the end, we will prove the following theorem.

THEOREM 4.1 (unique reconstruction of K). *Let $\sigma \in \mathcal{A}_\sigma$ and $K \in \mathcal{A}_K$. The map Λ_K uniquely determines $K(x,v,v')$. In particular, for any (x,v,v'), by a proper choice of ϕ and ψ, one can explicitly express $K(x,v,v')$ in terms of $M_\psi(\rho_\phi)$ with ρ_ϕ being the density associated with f_ϕ that solves* (1.1).

Note that K is the tumbling kernel, so the reconstruction necessarily needs at least one scatter. To do so, we decompose f into three, instead of two, parts. Let $f_\phi = f_{\phi,0} + f_{\phi,1} + f_{\phi,\geq 2}$, where $f_{\phi,0}$ solves (3.1) using ϕ as the initial data, and $f_{\phi,1}$ and $f_{\phi,\geq 2}$ solve the following:

$$\begin{cases} \partial_t f_{\phi,1} + v\cdot\nabla f_{\phi,1} &= -\sigma f_{\phi,1} + \mathcal{L}(f_{\phi,0}), \\ f_{\phi,1}(x,t=0,v) &= 0, \end{cases}, \tag{4.1}$$

and

$$\begin{cases} \partial_t f_{\phi,\geq 2} + v\cdot\nabla f_{\phi,\geq 2} &= -\sigma f_{\phi,\geq 2} + \mathcal{L}(f_{\phi,1} + f_{\phi,\geq 2}), \\ f_{\phi,\geq 2}(x,t=0,v) &= 0. \end{cases} \tag{4.2}$$

To reconstruct K, we will design a special set of test functions and initial conditions so as to have, in certain scenarios,

$$M_\psi(\rho_\phi) = M_\psi(\rho_{\phi,1}), \quad M_\psi(\rho_{\phi,0}) = 0 = M_\psi(\rho_{\phi,\geq 2}), \tag{4.3}$$

and the measurement $M_\psi(\rho_{\phi,1})$ is expected to give sufficient information to reconstruct K. Similarly to notations above, we omit the ϕ dependence in ρ and f when the context is clear.

As in the previous case, this will again hold in the limit as the initial data and measurement test functions become singular functions concentrated on initial velocity v_i and location x_i and measurement location x_m and time t_m, respectively.

Unlike in the previous case, we require x_m to avoid the line formed by $x_i + v_i t_m$ so as to ensure at least one scatter. This means we require the particle to initially travel with velocity v_i and change its direction to another $\hat{v}$ at a certain time $t_m - \hat{s}$. As such, the measurement location is chosen to be

$$x_m = x_m(t_m) = x_i + \hat{s}\hat{v} + (t_m - \hat{s})v_i \quad \text{with} \quad \hat{s} = \lambda t_m, \lambda \in (0,1), \hat{v} \in V \setminus \{v_i\}. \tag{4.4}$$

For the fixed tupel of (x_i, v_i, x_m, t_m), we should note that $\hat{s}, \hat{v}$ are uniquely determined, and there is a unique tumbling point at $(x_i + v_i(t_m - \hat{s}), \hat{v}, v_i)$ that contributes information to the measurement. See Figure 4.1.

Furthermore, by gradually shrinking t_m and $x_m - x_i$, the ellipse of observation shrinks, sustaining the geometry features, with $\hat{s}$ set to be a fixed fraction of t_m, pushing the tumbling point close to the starting point.

More specifically, let $\phi_x, \phi_v, \psi_x, \psi_t$ be defined as in (3.4), and we set $t_m := \varepsilon^\alpha$ for some $\alpha \in \left(\frac{3}{4}, 1\right)$, then we let

$$\phi(x,v) = \frac{1}{\varepsilon^3 \delta^2} \phi_x\left(\frac{x - x_i}{\varepsilon}\right) \phi_v\left(\frac{\mathbb{P}_{v_i}(v)}{\delta}\right) j(v; v_i) \qquad \in C_c^\infty, \tag{4.5}$$

$$\psi(x,t) = \frac{1}{\nu^3 \eta} \psi_x\left(\frac{x - x_m}{\nu}\right) \psi_t\left(\frac{t - t_m}{\eta}\right) C_{\hat{s},\hat{v}} \qquad \in C_c^\infty \tag{4.6}$$

for small scaling parameters $\varepsilon, \delta, \eta, \nu > 0$ and the constant

$$C_{\hat{s},\hat{v}} := \hat{s}^2(1 - \langle v_i, \hat{v} \rangle). \tag{4.7}$$

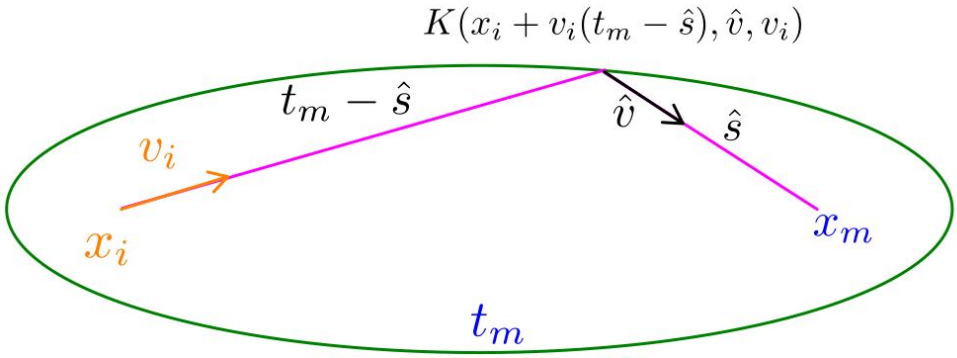

FIG. 4.1. *For a fixed $t_m > 0$, the ellipse with focal points x_i, x_m and radius t_m determines all points x with distance $\|x - x_i\| + \|x - x_m\| = t_m$. As v_i is given, the unique tumbling point $x_i + v_i(t_m - \hat{s})$ is the intersection of the half-line starting at x_i in direction v_i with this ellipse.*

Note that the scaling of ψ is different from the one in (3.5), in particular, the scalings of x are different in ϕ and ψ. We request $t_m = \varepsilon^\alpha \xrightarrow{\varepsilon\to 0} 0$. Note that ϵ is the rate at which ϕ is converging to a delta-measure in x. Since $\alpha < 1$, the convergence of the observation time $t_m \to 0$ is slightly slower than the convergence of the initial condition ϕ. Small time requirements are typical when observing the propagation of singularities; see, e.g., [13]. Here, we additionally made use of a particular relation between time and spatial scaling which will be beneficial to control the influence of the multiple tumble part $M_\psi(\rho_{\phi,\geq 2})$.

We claim for this setup, with t_m being very small, we will be able to achieve the estimate (4.3), and the measurement exactly reflects the value of $K(x_i + v_i(t_m - \hat{s}), \hat{v}, v_i)$, as seen in the following lemmas.

LEMMA 4.2. *Let σ be from the admissible set, and let the (ϕ, ψ) pairs be defined as in* (4.5)–(4.6)*, then $M_\psi(\rho_0)$ vanishes in the limit, meaning*

$$\lim_{\varepsilon\to 0} \lim_{\delta,\nu,\eta\to 0} M_\psi(\rho_0) = 0\,. \tag{4.8}$$

LEMMA 4.3. *Let K be from the admissible set, and let the initial data and test functions be as defined in* (4.5)–(4.6)*, then the measurement $M_\psi(\rho_1)$ reconstructs K, in the sense that*

$$\lim_{\varepsilon\to 0} \lim_{\delta,\nu,\eta\to 0} M_\psi(\rho_1) = K(x_i, \hat{v}, v_i)\,, \tag{4.9}$$

where $\hat{v}$ is the velocity after tumbling used in the construction of the measurement location x_m in (4.4).

LEMMA 4.4. *Assume K and σ are bounded and positive, then*

$$\lim_{\varepsilon\to 0} \lim_{\delta,\nu,\eta\to 0} M_\psi(\rho_{\geq 2}) = 0. \tag{4.10}$$

Together, these lemmas prove Theorem 4.1.

Proof of Theorem 4.1. Combining the previous three lemmas, in the limit (4.3) holds true, meaning

$$\lim_{\varepsilon\to 0} \lim_{\delta,\nu,\eta\to 0} M_\psi(\rho_f^\phi) = \lim_{\varepsilon\to 0} \lim_{\delta,\nu,\eta\to 0} M_\psi(\rho_1) = K(x_i, \hat{v}, v_i). \tag{4.11}$$ ∎

The rest of this section is dedicated to showing Lemmas 4.2, 4.3, and 4.4.

Lemma 4.2 states that the contribution from f_0 in the measurement vanishes as initial and measurement functions become singular. This is intuitively straightforward. Indeed, as illustrated in Figure 4.2, x_m is not along the straight line from x_i in the direction of v_i, so if ϕ is singular enough, x_m lies out of the support of f_0.

Proof of Lemma 4.2. Recalling the solution to (3.1) is in (3.8). If we test it with ψ, and make use of the change of variables $\tilde{t} = \frac{t-t_m}{\eta}$, $y = \frac{\mathbb{P}_{v_i}(v)}{\delta}$, and $\tilde{x} = \frac{x-x_m}{\varepsilon}$, we have

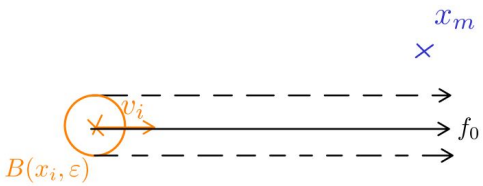

FIG. 4.2. *Considering the situation of a point measurement of f_0 at (x_m,t_m), where the initial velocity is prescribed as $\phi(x,v)=\tilde{\phi}(x)\delta_{v_i}(v)$, the support of $f_0(\cdot,t_m,v_i)$ equals $\operatorname{supp}\{\tilde{\phi}(x_i+v_it_m)\}\subset B(x_i+v_it_m,\varepsilon)$, the translated support of $\tilde{\phi}$. When ε becomes small, at some point $B(x_i+v_it_m,\varepsilon)$ no longer contains x_m, since $x_m\neq x_i+v_it_m$.*

$$
\begin{aligned}
M_\psi(\rho_0) &= \int_0^T \int_{\mathbb{R}^3} \int_V f_0(x,t,v)\,\mathrm{d}v\,\psi(x,t)\,\mathrm{d}x\,\mathrm{d}t \\
&= \frac{C_{\hat{s},\hat{v}}}{\varepsilon^3\delta^2\nu^3\eta}\int_0^T \int_{\mathbb{R}^3}\int_V e^{-\int_0^t \sigma(x-vs,v)\,\mathrm{d}s}\phi_x\left(\frac{x-vt-x_i}{\varepsilon}\right) \\
&\qquad \cdot \phi_v\left(\frac{\mathbb{P}_{v_i}(v)}{\delta}\right) j(v)\,\mathrm{d}v\,\psi_x\left(\frac{x-x_m}{\nu}\right)\psi_t\left(\frac{t-t_m}{\eta}\right)\mathrm{d}x\,\mathrm{d}t \\
&= \frac{C_{\hat{s},\hat{v}}}{\varepsilon^3}\int_{-\frac{t_m}{\eta}}^{\frac{T-t_m}{\eta}} \int_{\mathbb{R}^3}\int_{\mathbb{R}^2} e^{-\int_0^{t_m+\eta\tilde{t}}\sigma(x_m+\nu\tilde{x}-\mathbb{P}_{v_i}^{-1}(\delta y)s,\mathbb{P}_{v_i}^{-1}(\delta y))\,\mathrm{d}s}\phi_v(y) \\
&\qquad \cdot \phi_x\left(\frac{x_m+\nu\tilde{x}-\mathbb{P}_{v_i}^{-1}(\delta y)(t_m+\eta\tilde{t})-x_i}{\varepsilon}\right)\mathrm{d}y\,\psi_x(\tilde{x})\,\psi_t(\tilde{t})\,\mathrm{d}\tilde{x}\,\mathrm{d}\tilde{t} \\
&\xrightarrow{\delta,\nu,\eta\to 0} \frac{C_{\hat{s},\hat{v}}}{\varepsilon^3}e^{-\int_0^{t_m}\sigma(x_m-v_is,v_i)\,\mathrm{d}s}\phi_x\left(\frac{x_m-v_it_m-x_i}{\varepsilon}\right).
\end{aligned}
$$

In the last step, we exchange the limit with the integration using the dominated convergence theorem which is applicable because of the continuity of σ and ϕ_x. Noting the construction of x_m in (4.4),

$$
\left\|\frac{x_m-v_it_m-x_i}{\varepsilon}\right\| = \frac{\|\hat{s}(\hat{v}-v_i)\|}{\varepsilon} = \|\lambda(\hat{v}-v_i)\|\varepsilon^{\alpha-1} > 1
$$

for any small enough, but fixed, $\varepsilon>0$, making $\phi_x\left(\frac{x_m-v_it_m-x_i}{\varepsilon}\right)=0$ according to the definition of ϕ_x. This proves (4.8). ∎

Proof of Lemma 4.4. Repeating the arguments in the proof of Lemma 3.4, we estimate the remainder

$$
\begin{aligned}
M(\rho_{\geq 2}) &\leq \frac{1}{\varepsilon^3}C_K^2|V|e^{C_K|V|T}M\left(\int_0^t s\,\mathrm{d}s\right) = \frac{1}{\varepsilon^3}C\int_0^T\int_{\mathbb{R}^3} t^2\,\psi(x,t)\,\mathrm{d}x\,\mathrm{d}t\,C_{\hat{s},\hat{v}} \\
&= \frac{C}{\varepsilon^3}\tilde{C}\int_0^T t^2\frac{1}{\eta}\psi_t\left(\frac{t-t_m}{\eta}\right)\mathrm{d}t\,\hat{s}^2,
\end{aligned}
$$

where $C:=C_K^2|V|e^{C_K|V|T}/2$ and $\tilde{C}:=(1-\langle\hat{v},v_i\rangle)$ are positive constants and we used $f_1\leq tC_K\varepsilon^{-3}$, which can be seen in (3.12). We employ the dominated convergence theorem to the right-hand side to see

$$\lim_{\eta\to 0} M(\rho_{\geq 2}) \leq \frac{C}{\varepsilon^3}\tilde{C}t_m^2\hat{s}^2 = C\tilde{C}\lambda^2\varepsilon^{4\alpha-3} \xrightarrow{\varepsilon\to 0} 0,$$

because $\alpha > \frac{3}{4}$ was chosen. Together with the nonnegativity of $\rho_{\geq 2}$, we conclude (4.10). ∎

Lemma 4.3 lies at the core of Theorem 4.1, and the proof largely depends on explicit derivation. Noting that according to (4.4), with fixed (x_i, v_i) and (x_m, t_m), one finds a unique local point for the bacteria to tumble, $x_i + v_i(t_m - \hat{s})$, so the measurement should reflect K evaluated at this particular point.

Proof of Lemma 4.3. We first derive a closed form for f_1 by solving (4.1) along characteristics,

$$\begin{aligned} f_1(x,t,v) = \frac{1}{\varepsilon^3\delta^2}\int_0^t\int_V & e^{-\int_0^s \sigma(x-v\tau,v)\mathrm{d}\tau} K(x-vs,v,v') \\ & \cdot e^{-\int_0^{t-s}\sigma(x-vs-v'\tau,v')\,\mathrm{d}\tau}\phi_x\left(\frac{x-vs-v'(t-s)-x_i}{\varepsilon}\right) \\ & \cdot \phi_v\left(\frac{\mathbb{P}_{v_i}(v')}{\delta}\right) j(v';v_i)\,\mathrm{d}v'\,\mathrm{d}s\,, \end{aligned} \tag{4.12}$$

where we have used the explicit solution f_0 as in (3.8). Plugging it into the definition of the measurement,

$$\begin{aligned} M_\psi(\rho_1) &= \int_0^T\int_{\mathbb{R}^3}\int_V f_1(x,t,v)\,\mathrm{d}v\,\psi(x,t)\,\mathrm{d}x\,\mathrm{d}t \\ &= \int_0^T\int_{\mathbb{R}^3}\int_V\int_0^t\int_V \frac{C_{\hat{s},\hat{v}}}{\varepsilon^3\delta^2\nu^3\eta} e^{-\int_0^s\sigma(x-v\tau,v)\mathrm{d}\tau}K(x-vs,v,v') \\ &\quad \cdot e^{-\int_0^{t-s}\sigma(x-vs-v'\tau,v')\,\mathrm{d}\tau}\phi_x\left(\frac{x-vs-v'(t-s)-x_i}{\varepsilon}\right) \\ &\quad \cdot \phi_v\left(\frac{\mathbb{P}_{v_i}(v')}{\delta}\right) j(v')\mathrm{d}v'\,\mathrm{d}s\,\mathrm{d}v\,\psi_x\left(\frac{x-x_m}{\nu}\right)\psi_t\left(\frac{t-t_m}{\eta}\right)\mathrm{d}x\,\mathrm{d}t\,. \end{aligned}$$

Taking the limit and using dominant convergence theorem, we obtain

$$\begin{aligned} &\lim_{\delta,\nu,\eta\to 0} M_\psi(\rho_1) \\ &= \int_0^{t_m}\int_V \frac{C_{\hat{s},\hat{v}}}{\varepsilon^3} e^{-\int_0^s\sigma(x_m-v\tau,v)\mathrm{d}\tau}K(x_m-vs,v,v_i) \\ &\quad \cdot e^{-\int_0^{t_m-s}\sigma(x_m-vs-v_i\tau,v_i)\,\mathrm{d}\tau}\phi_x\left(\frac{x_m-vs-v_i(t_m-s)-x_i}{\varepsilon}\right)\mathrm{d}v\,\mathrm{d}s\,. \end{aligned} \tag{4.13}$$

The formula above could be further reduced if we notice the support condition for ϕ_x. In particular, if we denote the argument of ϕ_x, $\frac{x_m-vs-v_i(t_m-s)-x_i}{\varepsilon}$, to be $\mathfrak{a}$, it is straightforward to see that

$$\|\mathfrak{a}\| \geq \frac{\|x_m - x_o\| - s\|v-v_i\|}{\varepsilon}\,,$$

where we denote

$$x_o = x_i + v_i t_m\,, \tag{4.14}$$

the location of the particle at time t_m assuming it does not tumble. For small but fixed $\varepsilon > 0$, this further gives the following.

- When $s < c_1 := \frac{\|x_m - x_o\|}{4}$, since $\|v - v_i\| \le 2$,

$$\|\mathfrak{a}\| \ge \frac{\|x_m - x_o\| - 2s}{\varepsilon} = \frac{\|x_m - x_o\|}{2\varepsilon} > 1\,. \tag{4.15}$$

- When $\langle v_i, v\rangle > 1 - c_2 := 1 - \frac{\|x_m - x_o\|^2}{8t_m^2}$, since $\|v - v_i\| = \sqrt{2 - 2\langle v_i, v\rangle}$,

$$\|\mathfrak{a}\| > \frac{\|x_m - x_o\| - s\sqrt{2\frac{\|x_m - x_o\|^2}{8t_m^2}}}{\varepsilon} \ge \frac{\|x_m - x_o\|}{2\varepsilon} > 1\,. \tag{4.16}$$

That means that the integrand in (4.13) would be 0 due to the finite support of ϕ_x in these two parts of the domain.

In this reduced domain, $U = \{(s, v) \in [c_1, t_m] \times \{v \in V \mid \langle v, v_i\rangle \le 1 - c_2\}\}$, we define the function $\mathcal{S} : (s, v) \mapsto z := s(v - v_i)$. We note this function is injective. For fixed z in its image, we can calculate its inverse:

$$\mathcal{S}^{-1}(z) = (\zeta, \omega)(z) = \left(\frac{|z|^2}{2|\langle z, v_i\rangle|}, v_i + \frac{z}{\zeta(z)}\right). \tag{4.17}$$

So we conduct a change of variable by letting $z = \mathcal{S}(s, v)$, we further reduce the domain of (4.13) to $\mathcal{S}(U)$, and use the definition (4.7) of $C_{\hat{s},\hat{v}}$, to see that

$$\begin{aligned}
&\lim_{\delta,\nu,\eta\to 0} M_\psi(\rho_1)\\
&= \frac{1}{\varepsilon^3}\int_{\mathcal{S}(U)} e^{-\int_0^{\zeta(z)}\sigma(x_m - \tau\omega(z),\omega(z))\mathrm{d}\tau} K(x_m - \zeta(z)\omega(z), \omega(z), v_i)\\
&\qquad \cdot e^{-\int_0^{t_m-\zeta(z)}\sigma(x_m-\zeta(z)\omega(z)-v_i\tau,v_i)\,\mathrm{d}\tau}\phi_x\left(\frac{x_m - z - x_o}{\varepsilon}\right)\\
&\qquad \cdot \frac{\hat{s}^2}{\zeta(z)^2}\frac{1 - \langle v_i, \hat{v}\rangle}{1 - \langle v_i, \omega(z)\rangle}\,\mathrm{d}z\\
&= \int_{\frac{a-\mathcal{S}(U)}{\varepsilon}} e^{-\int_0^{\zeta(a-\varepsilon\tilde{z})}\sigma(x_m-\tau\omega(a-\varepsilon\tilde{z}),\omega(a-\varepsilon\tilde{z}))\mathrm{d}\tau}\\
&\qquad \cdot K(x_m - \zeta(a - \varepsilon\tilde{z})\omega(a - \varepsilon\tilde{z}), \omega(a - \varepsilon\tilde{z}), v_i)\\
&\qquad \cdot e^{-\int_0^{t_m-\zeta(a-\varepsilon\tilde{z})}\sigma(x_m-\zeta(a-\varepsilon\tilde{z})\omega(a-\varepsilon\tilde{z})-v_i\tau,v_i)\,\mathrm{d}\tau}\phi_x(\tilde{z})\\
&\qquad \cdot \frac{\hat{s}^2}{\zeta(a - \varepsilon\tilde{z})^2}\frac{1 - \langle v_i, \hat{v}\rangle}{1 - \langle v_i, \omega(a - \varepsilon\tilde{z})\rangle}\,\mathrm{d}\tilde{z},
\end{aligned}$$

where we used the determinent of the Jacobian of $\mathcal{S}$ being $s^2(1 - \langle v, v_i\rangle)$, and the substitution $\tilde{z} = \frac{a-z}{\varepsilon}$ for $a := x_m - x_o$ in the last step. For a visualization of the quantities, see Figure 4.3. The fact that a small ball around a with radius of order ε^α is contained in $\mathcal{S}(U)$ for every ε ensures that $\frac{a-\mathcal{S}(U)}{\varepsilon}$ will eventually contain the full support $B(0, 1)$ of ϕ_x for small ε; see Figure 4.4. Together with the continuity of K, σ, ζ, ω, this allows the application of the dominated convergence theorem,

$$\lim_{\delta,\nu,\eta\to 0} M_\psi(\rho_1) \xrightarrow{\varepsilon\to 0} K(x_i, \hat{v}, v_i)\int_{B(0,1)}\phi_x(\tilde{z})\,\mathrm{d}\tilde{z} = K(x_i, \hat{v}, v_i),$$

where we used the form (4.17) of ζ, ω to see $\zeta(a - \varepsilon\tilde{z})/\hat{s} \to 1$ while $\omega(a - \varepsilon\tilde{z}) \to \hat{v}$. ∎

Remark 4.5. The proof for all three lemmas are local-in-time, in the sense that the measurement time is converging to 0. This means that we can easily extend the result to deal with time dependent K as well. Suppose $K(x, t, v, v')$ should be recovered for a specific t value, then a new experiment is started at time t, meaning both the initial data ϕ and the measurements ψ should be prepared at reference time t.

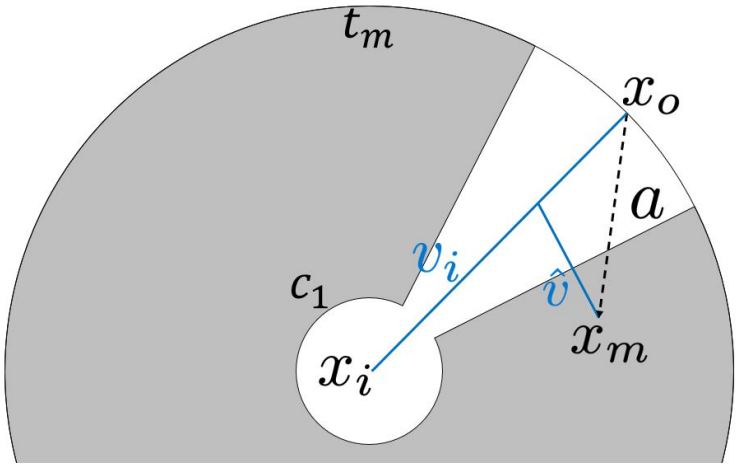

FIG. 4.3. *Geometry and quantities used in the proof, displayed in* 2 *dimensions* (2*D*). *In this figure,* $x_o = x_i + v_i t_m$, *the location of the particle assuming it does not tumble; see definition* (4.14). *Note that* t_m *is the length between* x_i *and* x_o. *The gray area is* $x_i + vs$ *for* $(s, v) \in U$. *This is the annulus* A *in Figure* 4.4(a) *translated by* x_i.

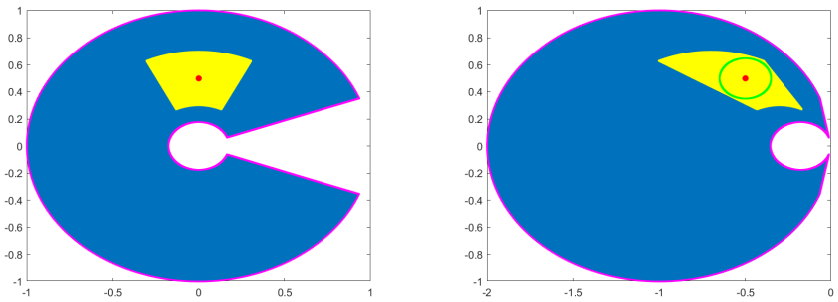

(a) Sliced annulus A. (b) Image of $\mathcal{S}(U)$.

FIG. 4.4. *Perturbation of* U *by* $\mathcal{S}$ *in* 2*D*. *In a first step,* $A := \{vs \mid (v, s) \in U\}$ *is displayed. The red dot marks* $\hat{v}\hat{s}$ *which is bounded away from the boundaries of* A *by construction. The yellow slice of an annulus is a neighborhood of* $\hat{v}\hat{s}$ *that is bounded by the arches of two circles. The image of* $\mathcal{S}(U)$ *is obtained by shifting each point in* $vs \in A$ *by* $-v_i s$. *In this picture, the red dot is* $a = \mathcal{S}(\hat{s}, \hat{v})$. *The image of the yellow area is bounded by the same arches of the circles, but the circles were shifted in direction* $-v_i$ *such that they touch* 0. *One can choose the yellow slice of the annulus large enough such that a ball with radius of order* ε^α*—whose boundary is depicted in green—is contained in the yellow image area.*

5. Conclusions. In this paper we work on a classical kinetic chemotaxis model, and give a rigorous proof for using density measurement to reconstruct tumbling and damping coefficients. As stated in the introduction, chemotaxis, as a mathematical biology subject, has attracted extensive research. There are abundant models. What we consider in this paper is a mere showcase of one of them (1.1) derived from the study of biased random walks [1]. In this specific setting, we show that when given a special design of initial data, the population density, one specific macroscopic quantity as a function of time, contains sufficient information to recover the microscopic quantities, such as the velocity tumbling kernel and its associated damping coefficient.

There are many new directions that are left unexplored, and we list a few here:

- Resultwise: In the current paper we only evaluate the uniqueness of the reconstruction but not the stability. Indeed, as concluded in Lemma 3.3, the reconstruction of σ requires differentiating the data. The stability of this reconstruction is thus expected to be bad in the L_∞ norm if the data are also assumed to be in C. A proper norm that is higher than C^1 needs to be selected to obtain a good stability. How the details are involved is a nontrivial task. We leave the discussion for stability for future work.
- Modelwise: We only showcase unique reconstruction for a very specific setting. More complicated models are not yet considered. We list a couple of possible directions below:
  - we only consider the well-controlled case when the space distribution of stimuli is fixed. But in practice, bacteria interact with the environment, and may provide self-attraction or self-repulsion. This changes the chemical concentration and leads to some interesting patterns; see [31, 32] and references therein. Mathematically, it is a convention to couple the chemotaxis equation (1.1) with an elliptic or parabolic equation for the chemical signal [7, 8, 9, 10]. However, it is almost impossible to trace the bacteria trajectory and measure the time dynamics of chemical concentration simultaneously. This prevents the quantification of most chemotaxis models except for some tightly controlled case [17, 18, 23] or well studied species [25, 36]. It would be interesting to study if the techniques presented in the current paper can be extended to the above-mentioned more complicated settings;
  - more sophisticated kinetic chemotaxis models have been proposed in the literature. For example, models that incorporate birth/death processes [29, 30], the tumbling time [22], or the adaptation process with internal variables [15, 35, 41, 42]. It would be interesting to investigate whether macroscopic quantities can provide enough information to recover the microscopic parameters for these more sophisticated kinetic models.

Despite its obvious significance, the inverse problem in mathematical biology is still in its infancy. Many related problems are left unaddressed. In the framework of kinetic formulation for bacteria-motion, a singular decomposition technique has demonstrated its flexibility and is very compatible with the kinetic formulation in the inverse problem setting. We expect to further investigate various problems listed above along this direction.

Acknowledgments. We would like to thank Marlies Pirner for the inspiring discussions that influenced the design of Lemma 3.6. We also thank Benoît Perthame for insightful comments regarding this work.

REFERENCES

[1] W. Alt, *Biased random walk models for chemotaxis and related diffusion approximations*, J. Math. Biol., 9 (1980), pp. 147–177, https://doi.org/10.1007/BF00275919.

[2] G. Bal, *Inverse transport theory and applications*, Inverse Problems, 25 (2009), 053001, https://doi.org/10.1088/0266-5611/25/5/053001.

[3] G. Bal and A. Jollivet, *Stability for time-dependent inverse transport*, SIAM J. Math. Anal., 42 (2010), pp. 679–700, https://doi.org/10.1137/080734480.

[4] G. Bal and A. Jollivet, *Generalized stability estimates in inverse transport theory*, Inverse Probl. Imaging, 12 (2018), pp. 59–90, https://doi.org/10.3934/ipi.2018003.

[5] G. Bal, I. Langmore, and F. Monard, *Inverse transport with isotropic sources and angularly averaged measurements*, Inverse Probl. Imaging, 2 (2008), pp. 23–42, https://doi.org/10.3934/ipi.2008.2.23.

[6] G. Bal and F. Monard, *Inverse transport with isotropic time-harmonic sources*, SIAM J. Math. Anal., 44 (2012), pp. 134–161, https://doi.org/10.1137/11083397X.

[7] N. Bournaveas and V. Calvez, *Critical mass phenomenon for a chemotaxis kinetic model with spherically symmetric initial data*, Ann. Inst. H. Poincare Anal. Non Linéaire, 26 (2009), pp. 1871–1895, https://doi.org/10.1016/j.anihpc.2009.02.001.

[8] N. Bournaveas, V. Calvez, S. Gutierrez, and B. Perthame, *Global existence for a kinetic model of chemotaxis via dispersion and Strichartz estimates*, Comm. Partial Differential Equations, 33 (2007), pp. 79–95, https://doi.org/10.1080/03605300601188474.

[9] F. Chalub, P. Markowich, B. Perthame, and C. Schmeiser, *Kinetic models for chemotaxis and their drift-diffusion limits*, Monatsh. Math., 142 (2004), pp. 123–141, https://doi.org/10.1007/s00605-004-0234-7.

[10] F. Chalub and J. F. Rodrigues, *A class of kinetic models for chemotaxis with threshold to prevent overcrowding*, Port. Math., 63 (2006), p. 227, http://eudml.org/doc/53089.

[11] K. Chen, Q. Li, and L. Wang, *Stability of inverse transport equation in diffusion scaling and Fokker–Planck limit*, SIAM J. Appl. Math., 78 (2018), pp. 2626–2647, https://doi.org/10.1137/17M1157969.

[12] M. Choulli and P. Stefanov, *Reconstruction of the coefficients of the stationary transport equation from boundary measurements*, Inverse Problems, 12 (1996), pp. L19–L23, https://doi.org/10.1088/0266-5611/12/5/001.

[13] M. Doumic, M. Escobedo, and M. Tournus, *An Inverse Problem: Recovering the Fragmentation Kernel from the Short-Time Behaviour of the Fragmentation Equation*, preprint, https://hal.science/hal-03494439v2.

[14] H. Egger, J.-F. Pietschmann, and M. Schlottbom, *Identification of chemotaxis models with volume-filling*, SIAM J. Appl. Math., 75 (2015), pp. 275–288, https://doi.org/10.1137/140967222.

[15] R. Erban and H. G. Othmer, *From individual to collective behavior in bacterial chemotaxis*, SIAM J. Appl. Math., 65 (2004), pp. 361–391, https://doi.org/10.1137/S0036139903433232.

[16] K. R. Fister and M. L. McCarthy, *Identification of a chemotactic sensitivity in a coupled system*, Math. Med. Biol., 25 (2008), pp. 215–232, https://doi.org/10.1093/imammb/dqn015.

[17] R. M. Ford and D. A. Lauffenburger, *Measurement of bacterial random motility and chemotaxis coefficients:* II. *Application of single-cell-based mathematical model*, Biotechnol. Bioeng., 37 (1991), pp. 661–672, https://doi.org/10.1002/bit.260370708.

[18] A. Giometto, F. Altermatt, A. Maritan, R. Stocker, and A. Rinaldo, *Generalized receptor law governs phototaxis in the phytoplankton euglena gracilis*, Proc. Nat. Acad. Sci. USA, 112 (2015), pp. 7045–7050, https://doi.org/10.1073/pnas.1422922112.

[19] H. Jeckel, E. Jelli, R. Hartmann, P. K. Singh, R. Mok, J. F. Totz, L. Vidakovic, B. Eckhardt, J. Dunkel, and K. Drescher, *Learning the space-time phase diagram of bacterial swarm expansion*, Proc. Nat. Acad. Sci. USA, 116 (2019), pp. 1489–1494, https://doi.org/10.1073/pnas.1811722116.

[20] C. Josenhans and S. Suerbaum, *The role of motility as a virulence factor in bacteria*, Int. J. Med. Microbiol., 291 (2002), pp. 605–614, https://doi.org/10.1078/1438-4221-00173.

[21] T. Julou, N. Desprat, D. Bensimon, and V. Croquette, *Monitoring microbial population dynamics at low densities*, Rev. Sci. Instrum., 83 (2012), 074301, https://doi.org/10.1063/1.4729796.

[22] L. Kanzler, C. Schmeiser, and V. Tora, *Two kinetic models for non-instantaneous binary alignment collisions*, Kinet. Relat. Models, (2023), https://doi.org/10.3934/krm.2023038.

[23] A. M. J. Law and M. D. Aitken, *Continuous-flow capillary assay for measuring bacterial chemotaxis*, Appl. Environ. Microbiol., 71 (2005), pp. 3137–3143, https://doi.org/10.1128/AEM.71.6.3137-3143.2005.

[24] Q. Li and W. Sun, *Applications of kinetic tools to inverse transport problems*, Inverse Problems, 36 (2020), 035011, https://doi.org/10.1088/1361-6420/ab59b8.

[25] Z. Li, Q. Cai, X. Zhang, G. Si, Q. Ouyang, C. Luo, and Y. Tu, *Barrier crossing in escherichia coli chemotaxis*, Phys. Rev. Lett., 118 (2017), 098101, https://doi.org/10.1103/PhysRevLett.118.098101.

[26] C. Liu, C. Zhou, W. Wang, and H. P. Zhang, *Bimetallic microswimmers speed up in confining channels*, Phys. Rev. Lett., 117 (2016), 198001, https://doi.org/10.1103/PhysRevLett.117.198001.

[27] A. Majorana, *Existence and uniqueness of positive solutions to a linear transport equation in a metric space*, Appl. Math. Lett., 10 (1997), pp. 49–53, https://doi.org/10.1016/S0893-9659(97)00104-3.

[28] N. M. Oliveira, K. R. Foster, and W. M. Durham, *Single-cell twitching chemotaxis in developing biofilms*, Proc. Nat. Acad. Sci. USA, 113 (2016), pp. 6532–6537, https://doi.org/10.1073/pnas.1600760113.

[29] H. Othmer, S. Dunbar, and W. Alt, *Models of dispersal in biological systems*, J. Math. Biol., 26 (1988), pp. 263–298, https://doi.org/10.1007/BF00277392.

[30] H. G. Othmer and T. Hillen, *The diffusion limit of transport equations* ii*: Chemotaxis equations*, SIAM J. Appl. Math., 62 (2002), pp. 1222–1250, https://doi.org/10.1137/S0036139900382772.

[31] K. J. Painter, *Mathematical models for chemotaxis and their applications in self-organisation phenomena*, J. Theoret. Biol., 481 (2019), pp. 162–182, https://doi.org/10.1016/j.jtbi.2018.06.019.

[32] B. Perthame and S. Yasuda, *Stiff-response-induced instability for chemotactic bacteria and flux-limited Keller–Segel equation*, Nonlinearity, 31 (2018), pp. 4065–4089, https://doi.org/10.1088/1361-6544/aac760.

[33] K. Ren, *Recent developments in numerical techniques for transport-based medical imaging methods*, Commun. Comput. Phys., 8 (2010), pp. 1–50, https://global-sci.org/intro/article_detail/cicp/7562.html.

[34] M. Salek, F. Carrara, V. Fernandez, J. Guasto, and R. Stocker, *Bacterial chemotaxis in a microfluidic t-maze reveals strong phenotypic heterogeneity in chemotactic sensitivity*, Nature Commun., 10 (2019), 1877, https://doi.org/10.1038/s41467-019-09521-2.

[35] G. Si, M. Tang, and X. Yang, *A pathway-based mean-field model for e. coli chemotaxis: Mathematical derivation and its hyperbolic and parabolic limits*, Multiscale Model. Simul., 12 (2014), pp. 907–926, https://doi.org/10.1137/130944199.

[36] G. Si, T. Wu, Q. Ouyang, and Y. Tu, *Pathway-based mean-field model for escherichia coli chemotaxis*, Phys. Rev. Lett., 109 (2012), 048101, https://doi.org/10.1103/PhysRevLett.109.048101.

[37] R. Singh and M. S. Olson, *Application of bacterial swimming and chemotaxis for enhanced bioremediation*, in Emerging Environmental Technologies, Springer, Dordrecht, Netherlands, 2008, pp. 149–172, https://doi.org/10.1007/978-1-4020-8786-8_7.

[38] P. Stefanov and Y. Zhong, *Inverse boundary problem for the two photon absorption transport equation*, SIAM J. Math. Anal., 54 (2022), pp. 2753–2767, https://doi.org/10.1137/21M1417387.

[39] J.-M. Swiecicki, O. Sliusarenko, and D. B. Weibel, *From swimming to swarming: Escherichia coli cell motility in two-dimensions*, Integrat. Biol., 5 (2013), pp. 1490–1494, https://doi.org/10.1039/c3ib40130h.

[40] R. T. Tranquillo, S. H. Zigmond, and D. A. Lauffenburger, *Measurement of the chemotaxis coefficient for human neutrophils in the under-agarose migration assay*, Cell Motility, 11 (1988), pp. 1–15, https://doi.org/10.1002/cm.970110102.

[41] C. Xue and H. G. Othmer, *Multiscale models of taxis-driven patterning in bacterial populations*, SIAM J. Appl. Math., 70 (2009), pp. 133–167, https://doi.org/10.1137/070711505.

[42] X. Xue and M. Tang, *Individual based models exhibiting Lévy-flight type movement induced by intracellular noise*, J. Math. Biol., 83 (2021), 27, https://doi.org/10.1007/s00285-021-01651-w.

[43] S. Yang, M. Huang, Y. Zhao, and H. P. Zhang, *Controlling cell motion and microscale flow with polarized light fields*, Phys. Rev. Lett., 126 (2021), 058001, https://doi.org/10.1103/PhysRevLett.126.058001.

[44] H. Zhao and Y. Zhong, *Instability of an inverse problem for the stationary radiative transport near the diffusion limit*, SIAM J. Math. Anal., 51 (2019), pp. 3750–3768, https://doi.org/10.1137/18M1222582.